INORGANIC CHEMISTRY FRONTIERS

RESEARCH ARTICLE

View Article Online
View Journal | View Issue

Cite this: *Inorg. Chem. Front.*, 2022, **9**, 5016

Direct synthesis of a stable radical doped electrically conductive coordination polymer†

Yong Yan,[a] Ning-Ning Zhang,*[b] Lisa Marie Tauche,[c] Kavipriya Thangavel,[c] Andreas Pöppl[c] and Harald Krautscheid*[a]

Received 3rd June 2022,
Accepted 11th August 2022

DOI: 10.1039/d2qi01180h

rsc.li/frontiers-inorganic

Radical coordination polymers exhibit tremendous potential in many areas. However, stable radical ligands are still rare and the syntheses of radical ligand derived coordination polymers are mainly limited to liquid diffusion based methods. Therefore, further exploration of new types of stable radical coordination polymers is strongly desired. Herein, we report on an NDI-based coordination polymer, $[K_2(ONDI)]_\infty$ (**K-ONDI**), which is synthesized directly by solvothermal reaction and exhibits radical properties and high stability in air as well as in common organic solvents. The $NDI^{\bullet-}$ radicals in **K-ONDI** are supposed to originate from electron transfer to the $ONDI^{2-}$ ligand under solvothermal conditions. Furthermore, benefitting from continuous π-stacking of the ligand in the crystal structure and unpaired electrons from $NDI^{\bullet-}$, **K-ONDI** shows intriguing semiconductive behaviour with an electrical conductivity value of 10^{-6} S cm^{-1}.

Introduction

Owing to potential applications in the fields of magnetic[1] or optical materials,[2] catalysts,[3] and electrical energy storage,[4] radical coordination polymers (RCPs) have attracted huge attention recently. Unfortunately, although RCPs exhibit intriguing potential, their radical states usually are not stable in air because of the high reactivity of ligands with unpaired electrons. In most cases, RCPs are sensitive to oxygen and need handling in inert atmosphere. In order to obtain stable RCPs, radical ligands with good stability have been introduced, *e.g.*, *N*-oxyl derivatives,[3] perchlorotriphenylmethyl,[5] and tetracyanoquinodimethane (TCNQ) derivatives.[1] However, available and stable radical ligands are still rare until now.[6] In addition, it is hard to maintain stability for most radical ligands under solvothermal conditions that are used widely for coordination polymers synthesis. The synthesis methods of RCPs are mainly limited to liquid diffusion.[1,5] Exploration of new types of stable RCPs is still a challenge.

Besides synthesis from radical ligands, RCPs can also be obtained by reducing or oxidizing redox-active coordination polymers.[7] In comparison to the limited number of radical ligands, neutral redox-active molecules that can form radical states under specific conditions are more easily accessible. Naphthalenediimides (NDI) are well known redox-active compounds featuring large planar structures with extended π-electron systems[8a,b] and have been widely used to design multifunctional coordination polymers, such as photochromic or electrochromic materials, sensors, and energy storage and conversion materials.[8c,d] Until now, radical character of coordination polymers based on NDI derived ligands was mainly generated by post-synthetic treatment like photo irradiation or reduction by chemical reagents.[9] Direct syntheses of NDI based radical coordination polymers are limited to electrochemical method.[10] Besides, the radical state of most NDI based coordination polymers does not remain for a long time because of easy re-oxidation of the $NDI^{\bullet-}$ core when exposed to air,[9c] which limits their potential applications. Further exploration of direct synthesis of stable radical NDI based coordination polymers is desired.

According to literature,[11] coordination bonds and π–π interactions, as two kinds of non-covalent interactions, are favourable for stabilizing radicals. It is well known that in the $NDI^{\bullet-}$ radical anion, the unpaired electron is delocalized over the naphthalene core structure and even extends into substituents on the nitrogen atoms in some cases.[8c,12] If the NDI core can coordinate to metal ions directly, the radical state of $NDI^{\bullet-}$ might be stabilized. However, in most cases the NDI core was only taken as a redox-active moiety and not directly engaged in

[a]*Fakultät für Chemie und Mineralogie, Institut für Anorganische Chemie, Universität Leipzig, Johannisallee 29, 04103 Leipzig, Germany.*
E-mail: Krautscheid@rz.uni-leipzig.de
[b]*School of Chemistry and Chemical Engineering, Liaocheng University, Liaocheng 252059, P. R. China. E-mail: zhangningning@lcu.edu.cn*
[c]*Felix Bloch Institute for Solid State Physics, Universität Leipzig, Linnéstraße 5, 04103 Leipzig, Germany*

†Electronic supplementary information (ESI) available: Additional tables and Fig. S1–S22. CCDC 2153468. For ESI and crystallographic data in CIF or other electronic format see DOI: https://doi.org/10.1039/d2qi01180h

coordination to metal ions.[7b] Recently, we found that the *N*-hydroxy modified NDI ligand H_2ONDI (**H_2ONDI** = 2,7-dihydroxybenzo[*lmn*][3,8]phenanthroline-1,3,6,8(2*H*,7*H*)-tetraone) can be deprotonated and coordinate to metal ions *via* the hydroxamate and carbonyl groups of the NDI core.[13a] Besides, $ONDI^{2-}$ prefers to form π–π stacking structures when assembled with metal ions, which is also favourable for stabilizing radicals. This ligand has hardly been used for the synthesis of RCPs before.[13] Herein, we report on the NDI based coordination polymer $[K_2(ONDI)]_\infty$ (**K-ONDI**; $ONDI^{2-}$ = 2,7-dioxybenzo[*lmn*][3,8]phenanthroline-1,3,6,8(2*H*,7*H*)-tetraone) with radical properties that was synthesized directly in a solvothermal reaction. The radical species remain stable even when exposed to air for one month or upon immersing into common organic solvents for five days. Furthermore, the concentration of radicals in **K-ONDI** can be tuned by adjusting the synthesis temperature, and it thus exhibits interesting semiconductive behaviour with a moderate electrical conductivity reaching about 10^{-6} S cm^{-1}.

Results and discussion

Crystal structure

Single crystals of **K-ONDI** were obtained by solvothermal reaction of H_2ONDI with KBF_4 in a DMF/MeOH solvent mixture. Crystal structure analysis by X-ray diffraction reveals that **K-ONDI** crystallizes in space group $P2_1/n$ with two formula units per unit cell. Each K^+ ion is coordinated by seven O atoms from five ligand molecules. Each $ONDI^{2-}$ ligand bridges ten K^+ ions through four chelating hydroxamate groups, μ_2 coordination of carbonyl oxygen atoms, and μ_3 coordination of $N{-}O^-$ oxygen atoms (Fig. 1a and S1†), resulting in a dense 3D metal–organic network (Fig. 1c). This coordination mode of the ligand $ONDI^{2-}$ is observed for the first time.[13] Continuous intermolecular π–π interactions between adjacent $ONDI^{2-}$ ligands are found along the crystallographic *a* axis. The shortest distance between phenyl centroids is 3.582 Å (Fig. 1b); the distance between parallel naphthalene planes is 3.371 Å (Fig. 1b), close to the typical interplanar distance of 3.3 Å of NDI organic derivatives.[10,14] Intermolecular π–π interactions between neighbouring ligands can be clearly observed from the calculated gradient isosurfaces according to the method reported by Johnson *et al.* (Fig. S2†).[15] It is worth to mention that NDI based coordination polymers showing π–π stacking structures are rare.[10,13a] Such a ligand arrangement is beneficial for charge transport.

Optical absorption and EPR spectroscopy

Although the colour of H_2ONDI is light yellow and that of the mono-deprotonated species is brown, the as-synthesized **K-ONDI** is dark blue, the solid-state absorption spectrum covers the complete visible range (Fig. 2a). In general, alkaline metal ions do not contribute to optical absorption properties in organic–inorganic hybrids. The huge difference in absorption spectra of the ligand in its protonated state, H_2ONDI·DMA, and the coordination polymer implies that a new species with a broad absorption band should be present in **K-ONDI**.

In order to investigate the origin, the optical absorption spectrum of H_2ONDI in solution was recorded. The results show that the organic ligand dissolved in DMA displays a broad absorption band around 650 nm (Fig. 2b) accompanied by a colour change from light yellow to light blue when treated with an excess of tetrabutylammonium fluoride (TBAF) as a weak base. The EPR spectrum shows that a more concentrated

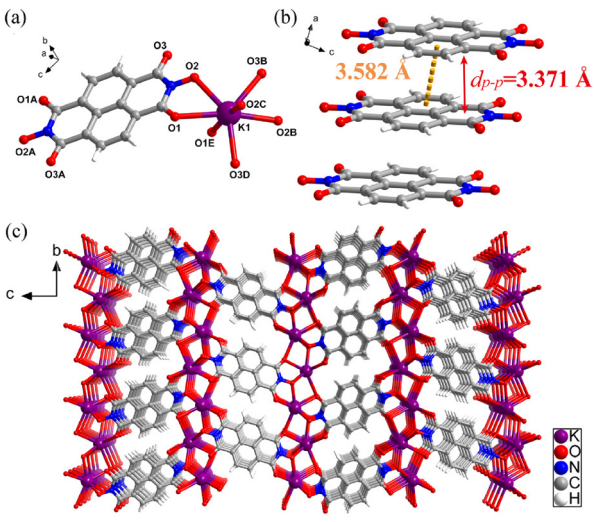

Fig. 1 Results of the single-crystal X-ray structure analysis of **K-ONDI**, (a) fragment of the **K-ONDI** network; (b) intermolecular π–π interactions between adjacent ligands (K^+ ions omitted); (c) view of the dense 3D network. Symmetry codes, A: 1 − *x*, 1 − *y*, 1 − *z*; B: −0.5 − *x*, −0.5 + *y*, 0.5 − *z*; C: 0.5 − *x*, −0.5 + *y*, 0.5 − *z*; D: *x*, −1 + *y*, *z*; E: −1 + *x*, *y*, *z*.

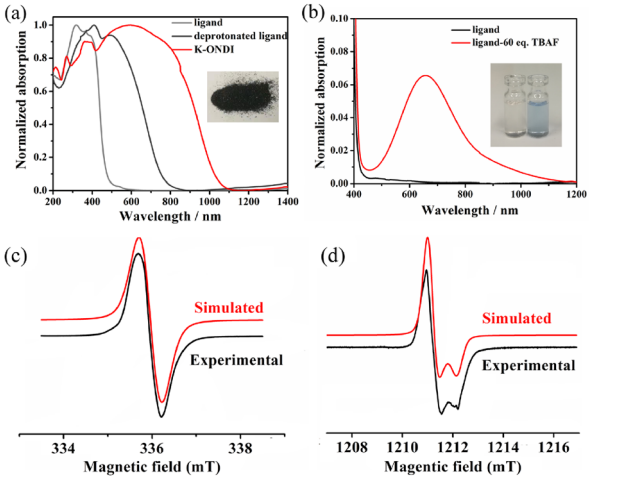

Fig. 2 (a) Solid-state absorption spectra of H_2ONDI·DMA, the mono-deprotonated species (Me_2NH_2)(HONDI), and **K-ONDI**; the inset shows the colour of **K-ONDI**; (b) the absorption spectrum of H_2ONDI dissolved in DMA (10^{-4} mol l^{-1}) changes upon adding 60 eq. tetrabutylammonium fluoride (TBAF); the inset displays the colour change of a solution after adding TBAF; (c) X-band and (d) Q-band solid state EPR spectra of **K-ONDI** and simulated radical signal.

blue solution (1.0×10^{-2} mol l^{-1}) exhibits an obvious unpaired electron signal (Fig. S3†). According to previous studies, the formation of $NDI^{\bullet-}$ radical anions can be induced by treatment with Lewis basic anions like F^-, CN^-, and OH^- accompanied by a colour change.[16] Therefore, the broad absorption band at 650 nm appearing in solution of H_2ONDI could be attributed to the formation of $NDI^{\bullet-}$ radical anions induced by F^-. As for **K-ONDI**, it not only shows a similar broad absorption band as H_2ONDI when treated with 60 eq. TBAF, but also displays a radical signal in its X-band EPR spectrum with a g factor of 2.0042(5) (Fig. 2c), close to values reported for $NDI^{\bullet-}$ radical anions in DMF solvent[17a] and in coordination polymers.[17b,c] A fit of the X-band EPR spectrum revealed a dominating Gaussian line shape with a line width of ΔB_{pp}^{G} = 0.43(2) mT with a small Lorentzian line width contribution of ΔB_{pp}^{L} = 0.16(2) mT. The obtained line widths are in agreement with previous reports of $NDI^{\bullet-}$ radical anions in coordination polymers.[17b,c] Moreover, Q-band EPR spectroscopy of **K-ONDI** revealed a small axial anisotropy of the g tensor with $g_{\perp}$ = 2.0044(2) and $g_{||}$ = 2.0026(2) and slightly smaller line widths ΔB_{pp}^{G} = 0.35(2) mT and ΔB_{pp}^{L} = 0.10(2) mT as compared to the X band spectra. An axially symmetric g tensor has been likewise reported for $NDI^{\bullet-}$ radical anions.[18] Therefore, it is reasonable to assign the observed EPR signal and the absorption band around 620 nm in **K-ONDI** to the $NDI^{\bullet-}$ radical anions. The absorption bands from 200 nm to 400 nm should be attributed to the π–π* transition of the organic ligand.[7a,19] Compared to **K-ONDI**, the $NDI^{\bullet-}$ absorption band of H_2ONDI in solution is slightly red-shifted, probably caused by the large polarity of the solvent DMA.

Since only the $NDI^{\bullet-}$ radical signal was detected by EPR and no other redox species were found in the solid state cyclic voltammogram of **K-ONDI** (Fig. S4†), intramolecular electron transfer can be excluded. According to literature, alkylamines, acting as electron donors, can induce $NDI^{\bullet-}$ formation by electron transfer.[20] Considering that Me_2NH is formed by hydrolytic decomposition of DMF,[21a] the $NDI^{\bullet-}$ present in **K-ONDI** may be generated by the alkylamine formed by decomposition of DMF under solvothermal conditions.

To verify this hypothesis, firstly, syntheses of **K-ODNI** were performed at different temperatures because higher temperature would promote the decomposition of DMF and, thus, produce more alkylamine which would be beneficial for the formation of $NDI^{\bullet-}$. The identical PXRD patterns demonstrate phase consistency of products obtained at 140, 150 and 160 °C (Fig. 3a). Also the solid-state UV-vis absorption spectra are very similar and exhibit broad $NDI^{\bullet-}$ absorption bands at 620 nm (Fig. 3b). Quantitative measurements of the numbers of spins in these three samples by EPR spectroscopy reveal 4.6×10^{14} mg^{-1} (140 °C), 1.2×10^{15} mg^{-1} (150 °C), and 4.9×10^{15} mg^{-1} (160 °C), the increasing concentration of radicals with increasing synthesis temperature (Fig. S5†) is consistent with the hypothesis that the decomposition products of DMF induce electron transfer to NDI leading to $NDI^{\bullet-}$ radicals.

Further, the solvent DMF was replaced with dimethylacetamide (DMA) and diethylformamide (DEF). DMA and DEF

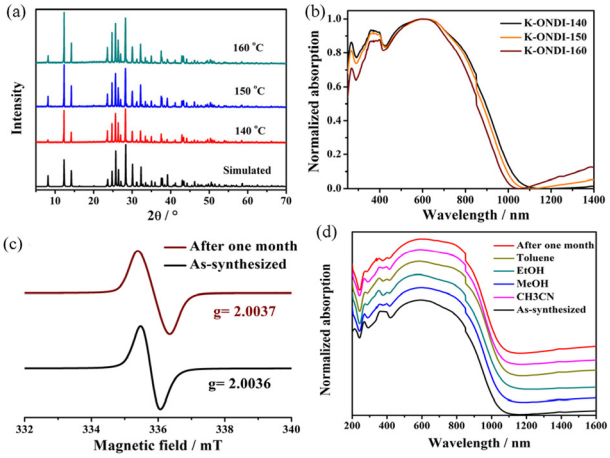

Fig. 3 PXRD patterns (a) and solid-state UV-vis absorption spectra (b) of **K-ONDI** synthesized at different temperatures; (c) Solid state EPR spectra of **K-ONDI** before and after exposure to air for one month; (d) solid-state optical absorption spectra of **K-ONDI** after exposure to air for one month and after immersing in organic solvents for five days.

both can produce respective alkylamines by hydrolysis during solvothermal reactions.[21] According to the PXRD patterns (Fig. S6a†), and solid-state UV-vis-infrared optical absorption spectra (Fig. S6b†), **K-ONDI** is obtained also with DMA or DEF. On the other hand, when DMF was replaced with DMSO, no solvothermal reaction could be observed because of the lack of organic bases (Fig. S7†). But in presence of triethylamine (Et_3N), **K-ONDI** was formed and the characteristic band of $NDI^{\bullet-}$ also appeared (Fig. S8†). This implies that Et_3N not only deprotonates the ligand, but also induces the formation of $NDI^{\bullet-}$. Since DMF, DMA and DEF can decompose to respective alkylamines under solvothermal conditions and $NDI^{\bullet-}$ doped **K-ONDI** can be obtained when using these solvents, it is reasonable to suggest that the formation of $NDI^{\bullet-}$ radicals in **K-ONDI** is related to the production of alkylamines by solvent decomposition.

Radical stability

K-ONDI synthesized at 140 °C exhibits good radical stability in air. After exposure to air for one month, the EPR radical signal still remains (Fig. 3c). The characteristic absorption band of the $NDI^{\bullet-}$ radical also still appears in the solid-state UV-vis-IR absorption spectra (Fig. 3d). In addition, the PXRD patterns show no obvious structural changes after contact to air for one month. On the other hand, **K-ONDI** also shows good stability in common organic solvents like MeOH, EtOH, CH_3CN, and toluene. After immersion in these solvents for five days, no changes were detected by PXRD (Fig. S9†). The absorption spectra of **K-ONDI** after the immersion process are nearly the same as those of the as-synthesized sample, which demonstrates the $NDI^{\bullet-}$ radical in **K-ONDI** is stable even in contact to the solvent. It is worth to mention that such air- and solvent-stable radical coordination polymers based on NDI derivatives are rare.[7] Consistent with previous studies,[11] the excellent

radical stability of **K-ONDI** combined with its structure features could be attributed to the synergistic interactions of the coordinative bonds of the NDI group and continuous π–π interactions between ligands.

Electronic structure calculation

Owing to the existence of continuous intermolecular π–π interactions between ligand molecules, effective orbitals overlap is reasonable to be expected. According to the results of DFT calculations, **K-ONDI** is a direct semiconductor. The calculated bandgap is 0.5 eV, which is in reasonable agreement with the experimentally determined optical gap of 1.27 eV (Fig. S10a†) because of the underestimation of bandgaps obtained from DFT calculations.[22] Combined with the κ point path in the Brillouin zone (Fig. S11†), the conduction band (CB) closest to the Fermi level is relatively flat along Z–Γ and B–D direction (Fig. 4), which indicates there is no effective orbital overlap between K^+ ions and organic ligands. The CB closest to the Fermi level shows a dispersion along Γ–Y, A–B, and D–E directions, with the dispersion width reaching about 0.18 eV (Fig. S12†). That means there is weak orbital overlap between adjacent columns of stacked ligands. Noticeably, the CB closest to the Fermi level significantly increases along Y–A direction and decreases along E–C direction. The dispersion widths between Y–A and E–C directions are about 0.36 eV. Such a big band dispersion is rare to be observed among coordination polymers[23] and demonstrates there is efficient orbital overlap. That corresponds to continuous π–π interactions along the *a* axis in the crystal structure. In contrast, the dispersions of the VB closest to the Fermi level are small (Fig. 4 and S12†), that means the electron mobility is expected to be bigger than the hole mobility in **K-ONDI**. Compared with the obvious VB dispersion in **Ca-ONDI** and **Sr-ONDI**,[13a] we suspect the π–π stacking structure of ligands may influence the band structure and charge carrier mobility.

From the analysis of density of states (DOS) and partial density of states (PDOS), the valence bands closest to the Fermi level largely consist of the states of O_α atoms (Fig. 4). The conduction band is mainly composed of the states of C atoms, with a small contribution from O_β. The contributions of N and K atoms to either occupied or unoccupied states near the Fermi level are nearly negligible.

Electrical conductivity

Due to the obvious radical signal and the crystal structure allowing efficient π orbital overlap, the electrical conductivity of **K-ONDI** (pressed pellets) obtained at different synthesis temperatures was measured using the two-probe method under direct current. The electrical conductivities of **K-ONDI** synthesized at different temperatures are 1.0×10^{-7} S cm^{-1} (140 °C), 4.3×10^{-7} S cm^{-1} (150 °C), and 6.5×10^{-6} S cm^{-1} (160 °C) (Fig. 5), respectively. This behaviour could be attributed to the increasing number of unpaired electrons (Fig. S5†). It is worth to mention that the electrical conductivity measured from pressed pellets is usually underestimated because of grain boundary resistance and sample anisotropy.[24] According to the single crystal structure data and theoretical calculation, the mechanism of electrical conductivity of **K-ONDI** could be assigned to band-like charge transport based on effective orbitals overlap originating in continuous intermolecular π–π interactions between organic ligands.[23b] On the other hand, considering the presence of grain boundary resistance in pressed pellets of a polycrystalline samples and possible defects caused by doped $NDI^{\bullet-}$, hopping charge transport may also contribute to the electrical conductivity of **K-ONDI**.[24a] According to previous studies,[25] the population of radical species in materials is important and proportional to their electrical conductivity. Compared to reported radical doped coordination polymers,[7a,25] **K-ONDI** exhibits a relatively high electrical conductivity even with less detected unpaired electrons (Table S2†), which probably is caused by an efficient charge transport path based on the π–π stacking structure.

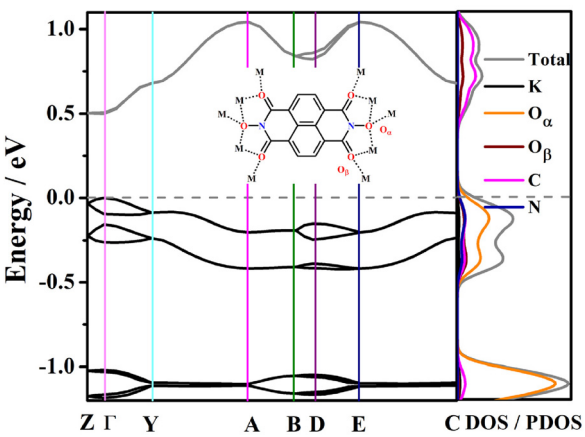

Fig. 4 The band structure and DOS/PDOS of **K-ONDI**. The dashed line represents the Fermi level (E_F).

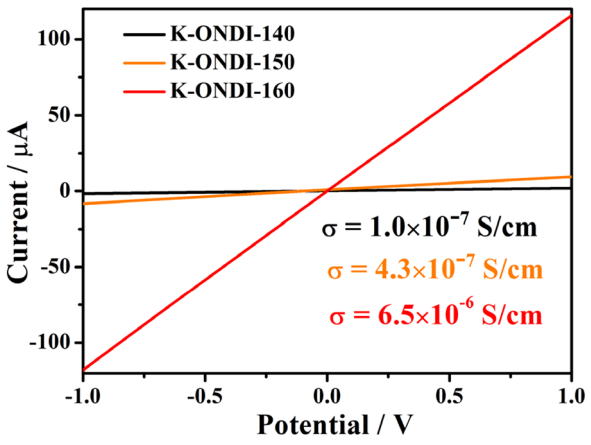

Fig. 5 *I–V* curve of **K-ONDI** synthesized at different temperatures (pressed pellet, two-probe method under ambient conditions, pellet thickness: **K-ONDI**-140, 0.70 mm; **K-ONDI**-150, 0.63 mm; **K-ONDI**-160, 0.72 mm; pellet diameter: 13 mm.

Measurements of the temperature dependent electrical conductivities of **K-ONDI** in the range of 25–80 °C (Fig. S22†) show that the electrical conductivity of **K-ONDI** increases with increasing temperature. The activation energies estimated from the slope ($\ln\sigma$ *vs.* $1/T$) in the linear range are 0.44, 0.42 and 0.15 eV for **K-ONDI** synthesized at 140, 150 and 160 °C, respectively.

Conclusions

In summary, we directly synthesized an NDI based coordination polymer with a significant and adjustable concentration of radical species by solvothermal reaction. This compound displays a strong radical EPR signal of $NDI^{\bullet-}$ that most likely is generated by electron transfer from amines, formed by decomposition of DMF under solvothermal conditions, to the NDI core of the ligand. Benefitting from its π–π stacking structure and coordination bonds to metal ions, **K-ONDI** exhibits good radical stability in air and common organic solvents. Due to efficient π orbitals overlap and unpaired electrons of $NDI^{\bullet-}$, **K-ONDI** shows a moderate electrical conductivity. Considering the wide applications of naphthalenediimide derivatives in coordination polymers, we believe that this work shows a new prospective to direct synthesis of radical doped CPs that would arouse interesting magnetic or electrical properties. Besides, this compound displays a broad optical absorption and semiconductive performance, which make it an ideal candidate for photo- or electrocatalysis.

Experimental

Materials and methods

All reagents were purchased commercially and used without further purification. 2,7-Dihydroxybenzo[*lmn*][3,8]phenanthroline-1,3,6,8(2*H*,7*H*)-tetraone (H_2ONDI) was synthesized according to a reported procedure.[13d] H_2ONDI·DMA and (Me_2NH_2) (HONDI) were prepared based on a reported method.[13a] Elemental analyses were carried out on a VARIO EL analyzer (Elementar). Thermogravimetric (TG) analyses were performed in Al_2O_3 crucibles on a NETZSCH STA 449 F1 thermal analyzer under Argon (50 ml min^{-1}) atmosphere at a heating rate of 10 K min^{-1}. Powder X-ray diffraction (PXRD) patterns were collected in Debye Scherrer mode on a STOE StadiP diffractometer using Cu-$K_{\alpha1}$ radiation (λ = 154.060 pm) at room temperature in the 2θ range of 5–80°. UV-Vis absorption spectra were collected on a Jasco V-670 UV–Vis–NIR spectrometer. IR spectra were measured on KBr pellets using a Bruker TENSOR 27 spectrometer.

Synthesis of K-ONDI. A mixture containing H_2ONDI (15 mg, 0.05 mmol) and KBF_4 (16 mg, 0.13 mmol), 2 mL DMF, and 2 mL CH_3OH was sealed in a Teflon lined autoclave and heated under autogenuous pressure to 140 °C for 1 day. Then the reaction mixture was cooled down to 30 °C within 10 hours. The obtained dark blue crystals were washed with DMA and CH_3OH several times. Yield 9 mg (*ca.* 50% based on ligand). Anal. calculated (%) for $K_2C_{14}H_4N_2O_6$ (M = 374.39 g mol^{-1}): C, 44.91; H, 1.08; N, 7.48. Found (%): C, 45.14; H, 0.99; N, 7.64.

X-ray crystallography

Single-crystal X-ray diffraction measurements were carried out on a STOE STADIVARI diffractometer equipped with an X-ray micro-source (Cu-Kα, λ = 154.186 pm) and a DECTRIS Pilatus 300k detector. The structure was solved by direct methods and refined using SHELX.[26] The hydrogen atoms of the ligand were added geometrically and refined using the riding model. The final structure was refined using a full-matrix least-squares refinement on F^2. All crystallographic calculations were performed within the Olex2 crystallographic software.[27]

Cyclic voltammetry

The solid-state cyclic voltammogram of **K-ONDI** was measured using a three-electrode cell at room temperature. About 5 mg of **K-ONDI** crystalline powder were milled and dispersed in 1 mL of ethanol. Two drops of the crystalline powder slurry were drop-cast onto the precleaned glassy carbon electrode and dried in air for the fabrication of the working electrode. Pt wire and Ag/Ag^+ act as the counter electrode and the reference electrode, respectively. Electrochemical measurements of the sample were carried out using a 0.1M $[(n\text{-}Bu)_4N]PF_6$ solution in acetonitrile under N_2 atmosphere. The reduction potentials of **K-ONDI** were obtained from the cyclic voltammogram and corrected with respect to the Fc/Fc^+ internal standard.

Electrical conductivity measurement

The conductivity of pressed pellets of **K-ONDI** (diameter 13 mm) was measured on a Biologic SP-150 instrument. The direct current–voltage (I–V) curves of **K-ONDI** pellets sandwiched between two silver gel coated hard plastic sheets (covered with Cu film on one side) electrodes were recorded under ambient conditions from −1 to +1 V. The specific electric conductivity σ is calculated by the expression $\sigma = \frac{I}{V} \times \frac{L}{\pi r^2}$, where L is the thickness and r the radius of the pellet. The values of I and V were obtained from the I–V curve. The temperature dependent conductivity measurement (Fig. S22†) was performed in an oven under ambient atmosphere. The temperature increased from room temperature to 80 °C in 2 h. The activation energy was calculated according to the Arrhenius equation: $\sigma = \sigma \cdot e^{-\frac{E_a}{K_B T}}$, where K_B is the Boltzmann constant and T represents the absolute temperature.

EPR measurements

EPR experiments of **K-ONDI** were performed on Bruker EMXmicro X-band and EMX Q-band spectrometers at room temperature, both equipped with cylindrical cavities. The X-band EPR spectrum of a solution of H_2ONDI in DMA was recorded using a flat cell in rectangular TE102 cavity. The EPR spectra were simulated using the MATLAB toolbox EasySpin.[28] Spin numbers were determined from the EPR spectra by

double integration and comparison with an ultramarine standard sample with known spin number.

Computation details

Calculation of intermolecular interactions: the plots of the electron density (ρ) and reduced density gradient ($s = 1/(2(3\pi^2)^{1/3})|\nabla\rho|/\rho^{4/3}$) of **K-ONDI** was obtained by density functional theory (DFT) calculations.[15] Calculations were performed with the B3LYP functional and the 6-311G (d,p) basis set,[29] using the Gaussian 16 program.[30] The results were analyzed by Multiwfn.[31]

The band structure and DOS were calculated using the CASTEP package.[32] The structural model for **K-ONDI** was directly taken from the single-crystal X-ray diffraction data. The exchange–correlation energy was described by the PBE functional within the GGA.[33] The norm conserving pseudopotentials were chosen to modulate the electron–ion interaction.[34] The plane-wave cutoff energy was 750 eV, and the threshold of 5×10^{-7} eV was set for the self-consistent field convergence of the total electronic energy. The Fermi level was selected as the reference and set to 0 eV by default. For the DOS/PDOS diagram a line broadening (smearing width) of 0.05 eV was used. Other parameters were set to default values.

Conflicts of interest

There are no conflicts to declare.

Acknowledgements

We gratefully acknowledge financial support from Deutsche Forschungsgemeinschaft (DFG), Universität Leipzig and the graduate school BuildMoNa. This work was also supported by the Open Foundation of State Key Laboratory of Structural Chemistry (20210009). The numerical calculations in this paper have been done on the Scientific Research Cloud Platform in School of Chemistry and Chemical Engineering, Liaocheng University. The authors, K. T. and A. P., gratefully acknowledge funding from the European Union's Horizon 2020 research and innovation programme under the Marie Skłodowska-Curie grant agreement No. 813209 entitled PARACAT.

Notes and references

1 (*a*) W. Kosaka, H. Fukunaga and H. Miyasaka, Electron-transferred donor/acceptor ferrimagnet with T_C = 91 K in a layered assembly of paddlewheel [Ru_2] units and TCNQ, *Inorg. Chem.*, 2015, **54**(20), 10001–10006; (*b*) J. Zhang, W. Kosaka, H. Sato and H. Miyasaka, Magnet creation by guest insertion into a paramagnetic charge-flexible layered metal–organic framework, *J. Am. Chem. Soc.*, 2021, **143**(18), 7021–7031; (*c*) J. Zhang and W. Kosaka, Kunihisa Sugimoto and H. Miyasaka, Magnetic sponge behaviour via electronic state modulations, *J. Am. Chem. Soc.*, 2018, **140**(16), 5644–5652.

2 (*a*) H. Liu, H. Qin, N. Shen, S. Yan, Y. Wang, X. Yin, X. Chen, C. Zhang, X. Dai, R. Zhou, X. Ouyang, Z. Chai and S. Wang, Emergence of a radical-stabilizing metal–organic framework as a radio-photoluminescence dosimeter, *Angew. Chem., Int. Ed.*, 2020, **59**, 15209–15214; (*b*) B. Lü, Y. Chen, P. Li, B. Wang, K. Müllen and M. Yin, Stable radical anions generated from a porous perylenediimide metal-organic framework for boosting near-infrared photothermal conversion, *Nat. Commun.*, 2019, **10**, 1–8.

3 (*a*) J. L. Zhuang, X. Y. Liu, Y. Zhang, C. Wang, H. L. Mao, J. Guo, X. Du, S. B. Zhu, B. Ren and A. Terfort, Zr-metal–organic frameworks featuring TEMPO radicals: synergistic effect between TEMPO and hydrophilic Zr-node defects boosting aerobic oxidation of alcohols, *ACS Appl. Mater. Interfaces*, 2019, **11**, 3034–3043; (*b*) K. M. Zwolinski and M. J. Chmielewski, TEMPO-appended metal–organic frameworks as highly active, selective, and reusable catalysts for mild aerobic oxidation of alcohols, *ACS Appl. Mater. Interfaces*, 2017, **9**, 33956–33967; (*c*) M. J. Jellen, M. J. Ayodele, A. Cantu, M. D. E. Forbes and M. A. Garcia-Garibay, 2D arrays of organic qubit candidates embedded into a pillared-paddlewheel metal–organic framework, *J. Am. Chem. Soc.*, 2020, **142**, 18513–18521.

4 (*a*) D. Sheberla, J. C. Bachman, J. S. Elias, C. J. Sun, Y. Shao-Horn and M. Dincă, Conductive MOF electrodes for stable supercapacitors with high areal capacitance, *Nat. Mat.*, 2017, **16**, 220–224; (*b*) J. Liu, X. Song, T. Zhang, S. Liu, H. Wen and L. Chen, 2D conductive metal–organic frameworks: an emerging platform for electrochemical energy storage, *Angew. Chem., Int. Ed.*, 2021, **60**, 5612–5624.

5 (*a*) D. Maspoch, D. Ruiz-Molina, K. Wurst, N. Doming, M. Cavallini, F. Biscarini, J. Tejada, C. Rovira and J. Veciana, A nanoporous molecular magnet with reversible solvent-induced mechanical and magnetic properties, *Nat. Mat.*, 2003, **2**, 190–195; (*b*) D. Maspoch, N. Domingo, D. Ruiz-Molina, K. Wurst, J. M. Hernández, G. Vaughan, C. Rovira, F. Lloret, J. Tejada and J. Veciana, Coexistence of ferro- and antiferromagnetic interactions in a metal–organic radical-based (6,3)-helical network with large channel, *Chem. Commun.*, 2005, 5035–5037; (*c*) A. Datcu, N. Roques, V. Jubera, D. Maspoch, X. Fontrodona, K. Wurst, I. Imaz, G. Mouchaham, J. P. Sutter, C. Rovira and J. Veciana, Three-dimensional porous metal–radical frameworks based on triphenylmethyl radicals, *Chem. – Eur. J.*, 2012, **18**, 152–162; (*d*) S. Kimura, M. Uejima, W. Ota, T. Sato, S. Kusaka, R. Matsuda, H. Nishihara and T. Kusamoto, An open-shell, luminescent, two-dimensional coordination polymer with a honeycomb lattice and triangular organic radical, *J. Am. Chem. Soc.*, 2021, **143**, 4329–4338; (*e*) S. Kimura, R. Matsuoka, S. Kimura, H. Nishihara and T. Kusamoto, Radical-based coordination polymers as a platform for magnetoluminescence, *J. Am. Chem. Soc.*, 2021, **143**, 5610–5615.

6 T. B. Faust and D. M. D'Alessandro, Radicals in metal–organic frameworks, *RSC Adv.*, 2014, **4**, 17498–17512.

7 (*a*) H. C. Wentz, G. Skorupskii, A. B. Bonfim, J. L. Mancuso, C. H. Hendon, E. H. Oriel, G. T. Sazamad and M. G. Campbell, Switchable electrical conductivity in a three-dimensional metal–organic framework via reversible ligand n-doping, *Chem. Sci.*, 2020, **11**, 1342–1346; (*b*) M. A. Gordillo, P. A. Benavides, D. K. Panda and S. Saha, The advent of electrically conducting double-helical metal–organic frameworks featuring butterfly-shaped electron-rich π-extended tetrathiafulvalene ligands, *ACS Appl. Mater. Interfaces*, 2020, **12**, 12955–12961; (*c*) H. Y. Wang, J. Y. Ge, C. Hua, C. Q. Jiao, Y. Wu, C. F. Leong, D. M. D'Alessandro, T. Liu and J. L. Zuo, Photo- and electronically switchable spin-crossover Iron(II) metal–organic frameworks based on a tetrathiafulvalene ligand, *Angew. Chem., Int. Ed.*, 2017, **56**, 5465–5470; (*d*) D. A. Haynes, L. J. van Laeren and O. Q. Munro, Cobalt porphyrin–thiazyl radical coordination polymers: toward metal–organic electronics, *J. Am. Chem. Soc.*, 2017, **139**, 14620–14637.

8 (*a*) M. Al Kobaisi, S. V. Bhosale, K. Latham, A. M. Raynor and S. V. Bhosale, Functional naphthalene diimides: synthesis, properties, and applications, *Chem. Rev.*, 2016, **116**, 11685–11796; (*b*) S. V. Bhosale, M. Al Kobaisi, R. W. Jadhav, P. P. Morajkar, L. A. Jones and S. George, Naphthalene diimides: perspectives and promise, *Chem. Soc. Rev.*, 2021, **50**, 9845–9998; (*c*) M. Pan, X. M. Lin, G. B. Li and C. Y. Su, Progress in the study of metal–organic materials applying naphthalene diimide (NDI) ligands, *Coord. Chem. Rev.*, 2011, **255**, 1921–1936; (*d*) Y. Zhou and L. Han, Recent advances in naphthalenediimide-based metal-organic frameworks: structures and applications, *Coord. Chem. Rev.*, 2021, **430**, 213665.

9 (*a*) L. Han, L. Qin, L. P. Xu, Y. Zhou, J. L. Sun and X. D. Zou, A novel photochromic calcium-based metal–organic framework derived from a naphthalene diimide chromophore, *Chem. Commun.*, 2013, **49**, 406–408; (*b*) B. Garai, A. Mallick and R. Banerjee, Photochromic metal–organic frameworks for inkless and erasable printing, *Chem. Sci.*, 2016, **7**, 2195–2200; (*c*) H. C. Wentz and M. G. Campbell, Fluoride detection with a redox-active naphthalene diimide metal–organic framework, *Polyhedron*, 2018, **154**, 309–313.

10 (*a*) L. Qu, H. Iguchi, S. Takaishi, F. Habib, C. F. Leong, D. M. D'Alessandro, M. Yamashita, H. Abe, E. Nishibori and M. Yamashita, Porous molecular conductor: electrochemical fabrication of through-space conduction pathways among linear coordination polymers, *J. Am. Chem. Soc.*, 2019, **141**, 6802–6806; (*b*) S. Koyama, T. Tanabe, S. Takaishi, M. Yamashita and H. Iguchi, Preliminary chemical reduction for synthesizing a stable porous molecular conductor with neutral metal nodes, *Chem. Commun.*, 2020, **56**, 13109–13112.

11 B. Tang, J. Zhao, J. F. Xu and X. Zhang, Tuning the stability of organic radicals: from covalent approaches to non-covalent approaches, *Chem. Sci.*, 2020, **11**, 1192–1204.

12 S. V. Bhosale, C. H. Jani and S. J. Langford, Chemistry of naphthalene diimides, *Chem. Soc. Rev.*, 2008, **37**, 331–342.

13 (*a*) Y. Yan, S. Henfling, N.–N. Zhang and H. Krautscheid, Semiconductive coordination polymers with continuous π–π interactions and defined crystal structures, *Chem. Commun.*, 2021, **57**, 10407–10410; (*b*) M. A. Houghton, A. Bilyk, M. M. Harding, P. Turner and T. W. Hambley, Effect of guest molecules, metal ions and linker length on the assembly of chiral [2 + 2] metallomacrocycles: solution studies and crystal structures, *J. Chem. Soc., Dalton Trans.*, 1997, 2725–2733; (*c*) L. Zhang, L. Lin, D. Liu, Y. J. Lin, Z. H. Li and G. X. Jin, Stacking interactions induced selective conformation of discrete aromatic arrays and Borromean rings, *J. Am. Chem. Soc.*, 2017, **139**, 1653–1660; (*d*) D. Liu, Y. Lu, Y. J. Lin and G. X. Jin, Donor–acceptor [2]- and [3] catenanes assembled from versatile pre-organized Cp*Rh/Ir-directed pseudorotaxane tectons, *Chem. – Eur. J.*, 2019, **25**, 14785–14789.

14 Y. Matsunaga, K. Goto, K. Kubono, K. Sako and T. Shinmyozu, Photoinduced color change and photomechanical effect of naphthalene diimides bearing alkylamine moieties in the solid state, *Chem. – Eur. J.*, 2014, **20**, 7309–7316.

15 E. R. Johnson, S. Keinan, P. Mori-Sánchez, J. Contreras-García, A. J. Cohen and W. T. Yang, Revealing Noncovalent Interactions, *J. Am. Chem. Soc.*, 2010, **132**, 6498–6506.

16 S. Saha, Anion-induced electron transfer, *Acc. Chem. Res.*, 2018, **51**, 2225–2236.

17 (*a*) G. Andric, J. F. Boas, A. M. Bond, G. D. Fallon, K. P. Ghiggino, C. F. Hogan, J. A. Hutchison, M. A.-P. Lee, S. J. Langford, J. R. Pilbrow, G. J. Troup and C. P. Woodward, Spectroscopy of naphthalene diimides and their anion radicals, *Aust. J. Chem.*, 2004, **57**, 1011–1019; (*b*) J. Z. Liao, C. Wu, X. Y. Wu, S. Q. Deng and C. Z. Lu, Exceptional photosensitivity of a polyoxometalate-based charge-transfer hybrid material, *Chem. Commun.*, 2016, **52**, 7394–7397; (*c*) J. Z. Liao, J. F. Chang, L. Meng, H. L. Zhang, S. S. Wang and C. Z. Lu, Lone pair-π interaction-induced generation of photochromic coordination networks with photoswitchable conductance, *Chem. Commun.*, 2017, **53**, 9701–9704.

18 Y. Beldjoudi, A. Narayanan, I. Roy, T. J. Pearson, M. M. Cetin, M. T. Nguyen, M. D. Krzyaniak, F. M. Alsubaie, M. R. Wasielewski, S. I. Stupp and J. F. Stoddart, Supramolecular tessellations by a rigid naphthalene diimide triangle, *J. Am. Chem. Soc.*, 2019, **141**, 17783–17795.

19 (*a*) J. Z. Liao, H. L. Zhang, S. S. Wang, J. P. Yong, X. Y. Wu, R. Yu and C. Z. Lu, Multifunctional radical-doped polyoxometalate-based host–guest material: photochromism and photocatalytic activity, *Inorg. Chem.*, 2015, **54**, 4345–4350; (*b*) K. Fuku, M. Miyata, S. Takaishi, T. Yoshida, M. Yamashita, N. Hoshino, T. Akutagawa, H. Ohtsu, M. Kawano and H. Iguchi, Emergence of electrical conductivity in a flexible coordination polymer by using chemical reduction, *Chem. Commun.*, 2020, **56**, 8619–8622.

20 (*a*) A. Mallick, B. Garai, M. A. Addicoat, P. S. Petkov, T. Heine and R. Banerjee, Solid state organic amine detection in a photochromic porous metal organic framework, *Chem. Sci.*, 2015, **6**, 1420–1425; (*b*) S. H. Lee, B. M. Oh, C. Y. Hong, S. K. Jung, S. H. Park, G. G. Jeon, Y. W. Kwon, S. Jang, Y. Lee, D. Kim, J. H. Kim and O. P. Kwon, Gas-induced ion-free stable radical anion formation of organic semiconducting solids as highly gas-selective probes, *ACS Appl. Mater. Interfaces*, 2019, **11**, 35904–35913.

21 (*a*) A. D. Burrows, K. Cassar, R. M. W. Friend, M. F. Mahon, S. P. Rigbyb and J. E. Warren, Solvent hydrolysis and templating effects in the synthesis of metal-organic frameworks, *CrystEngComm*, 2005, **7**, 548–550; (*b*) R. Seetharaj, P. V. Vandana, P. Arya and S. Mathew, Dependence of solvents, pH, molar ratio and temperature in tuning metal organic framework architecture, *Arabian J. Chem.*, 2019, **12**, 295–315.

22 (*a*) K. Burke, Perspective on density functional theory, *J. Chem. Phys.*, 2012, **136**, 150901; (*b*) M. Grüning, A. Marini and A. Rubio, Density functionals from many-body perturbation theory: the band gap for semiconductors and insulators, *J. Chem. Phys.*, 2006, **124**, 154108.

23 (*a*) A. Pathak, J. W. Shen, M. Usman, L. F. Wei, S. Mendiratta, Y. S. Chang, B. Sainbileg, C.-M. Ngue, R. S. Chen, M. Hayashi, T. T. Luo, F. R. Chen, K. H. Chen, T. W. Tseng, L. C. Chen and K. L. Lu, Integration of a (–Cu–S–)$_n$ plane in a metal–organic framework affords high electrical conductivity, *Nat. Commun.*, 2019, **10**, 1721–1728; (*b*) C. H. Hendon, A. J. Rieth, M. D. Korzyński and M. Dincă, Grand challenges and future opportunities for metal–organic frameworks, *ACS Cent. Sci.*, 2017, **3**, 554–563.

24 (*a*) L. S. Xie, G. Skorupskii and M. Dincă, Electrically conductive metal–organic frameworks, *Chem. Rev.*, 2020, **120**, 8536–8580; (*b*) G. Skorupskii, B. A. Trump, T. W. Kasel, C. M. Brown, C. H. Hendon and M. Dincă, Efficient and tunable one-dimensional charge transport in layered lanthanide metal–organic frameworks, *Nat. Chem.*, 2020, **12**, 131–136.

25 S. Zhang, D. K. Panda, A. Yadav, W. Zhou and S. Saha, Effects of intervalence charge transfer interaction between π-stacked mixed valent tetrathiafulvalene ligands on the electrical conductivity of 3D metal–organic frameworks, *Chem. Sci.*, 2021, **12**, 13379–13391.

26 G. M. Sheldrick, A short history of SHELX, *Acta Crystallogr., Sect. A: Found. Crystallogr.*, 2008, **64**, 112–122.

27 O. V. Dolomanov, L. J. Bourhis, R. J. Gildea, J. A. K. Howard and H. Puschmann, OLEX2: a complete structure solution, refinement and analysis program, *J. Appl. Crystallogr.*, 2009, **42**, 339–341.

28 S. Stoll and A. Schweiger, EasySpin, a comprehensive software package for spectral simulation and analysis in EPR, *J. Magn. Reson.*, 2006, **178**, 42–55.

29 C. T. Lee, W. T. Yang and R. G. Parr, Development of the Colle-Salvetti correlation-energy formula into a functional of the electron density, *Phys. Rev. B: Condens. Matter Mater. Phys.*, 1988, **37**, 785–789.

30 M. J. Frisch, G. W. Trucks, H. B. Schlegel, G. E. Scuseria, M. A. Robb, J. R. Cheeseman, G. Scalmani, V. Barone, G. A. Petersson, H. Nakatsuji, X. Li, M. Caricato, A. V. Marenich, J. Bloino, B. G. Janesko, R. Gomperts, B. Mennucci, H. P. Hratchian, J. V. Ortiz, A. F. Izmaylov, J. L. Sonnenberg, D. Williams-Young, F. Ding, F. Lipparini, F. Egidi, J. Goings, B. Peng, A. Petrone, T. Henderson, D. Ranasinghe, V. G. Zakrzewski, J. Gao, N. Rega, G. Zheng, W. Liang, M. Hada, M. Ehara, K. Toyota, R. Fukuda, J. Hasegawa, M. Ishida, T. Nakajima, Y. Honda, O. Kitao, H. Nakai, T. Vreven, K. Throssell, J. A. Montgomery Jr., J. E. Peralta, F. Ogliaro, M. J. Bearpark, J. J. Heyd, E. N. Brothers, K. N. Kudin, V. N. Staroverov, T. A. Keith, R. Kobayashi, J. Normand, K. Raghavachari, A. P. Rendell, J. C. Burant, S. S. Iyengar, J. Tomasi, M. Cossi, J. M. Millam, M. Klene, C. Adamo, R. Cammi, J. W. Ochterski, R. L. Martin, K. Morokuma, O. Farkas, J. B. Foresman and D. J. Fox, *Gaussian 16, Revision C.01*, Gaussian, Inc., Wallingford CT, 2016.

31 T. Lu and F. W. Chen, Multiwfn: a multifunctional wavefunction analyzer, *J. Comput. Chem.*, 2012, **33**, 580–592.

32 S. J. Clark, M. D. Segall, C. J. Pickard, P. J. Hasnip, M. I. J. Probert, K. Refson and M. C. Payne, First principles methods using CASTEP, *Z. Kristallogr. – Cryst. Mater.*, 2005, **220**, 567–570.

33 (*a*) B. Hammer, L. B. Hansen and J. K. Norskov, Improved adsorption energetics within density-functional theory using revised Perdew-Burke-Ernzerhof functionals, *Phys. Rev. B: Condens. Matter Mater. Phys.*, 1999, **59**, 7413–7421; (*b*) J. P. Perdew and Y. Wang, Accurate and simple analytic representation of the electron-gas correlation energy, *Phys. Rev. B: Condens. Matter Mater. Phys.*, 1992, **45**, 13244–13249.

34 (*a*) D. R. Hamann, M. Schlüter and C. Chiang, Norm-conserving pseudopotentials, *Phys. Rev. Lett.*, 1979, **43**, 1494–1497; (*b*) J. S. Lin, A. Qteish, M. C. Payne and V. Heine, Optimized and transferable nonlocal separable ab initio pseudopotentials, *Phys. Rev. B: Condens. Matter Mater. Phys.*, 1993, **47**, 4174–4180.